THE JOURNAL OF PHYSICAL CHEMISTRY C

C: Physical Processes in Nanomaterials and Nanostructures

Doped Colloidal InAs Nanocrystals in the Single Ionized Dopant Limit

Moussa Biaye, Yorai Amit, Kamil Gradkowski, Uri Banin, Natalia Turek, Sylvie Godey, Younes Makoudi, Dominique Deresmes, Athmane Tadjine, Christophe Delerue, and Thierry Mélin

J. Phys. Chem. C, **Just Accepted Manuscript** • DOI: 10.1021/acs.jpcc.9b02576 • Publication Date (Web): 16 May 2019

ACS Publications

is published by the American Chemical Society. 1155 Sixteenth Street N.W., Washington, DC 20036

Doped Colloidal InAs Nanocrystals in the Single Ionized Dopant Limit

*Moussa Biaye[1], Yorai Amit[2], Kamil Gradkowski[2,†], Uri Banin[2], Natalia Turek[1], Sylvie Godey[1], Younes Makoudi[1,‡], Dominique Deresmes[1], Athmane Tadjine[1], Christophe Delerue[1], Thierry Mélin[1,]**

(1) Institute of Electronics Microelectronics and Nanotechnology, University of Lille and Centre National de la Recherche Scientifique, IEMN-CNRS UMR 8520, Avenue Poincaré CS 60069, 59652 Villeneuve d'Ascq Cedex, France.

(2) Institute of Chemistry, Hebrew University, Jerusalem 91904, Israel ; Center for Nanoscience and Nanotechnology, Hebrew University, Jerusalem 91904, Israel.

* corresponding author : thierry.melin@iemn.fr

† present address: Photonic Packaging Group, Tyndall National Institute, Lee Maltings Complex, Cork T12R5CP, Ireland

‡ present address: Institut FEMTO-ST, CNRS, Université Bourgogne Franche-Comté, 15B Avenue des Montboucons, F-25030 Besançon Cedex, France.

ABSTRACT

We investigate the electronic properties of individual n-type (Cu) doped and p-type (Ag) doped InAs colloidal nanocrystals (NCs) in the 2-8 nm size range from their charge transfers towards a highly oriented pyrolytic graphite (HOPG) substrate, using ultra-high vacuum Kelvin probe force microscopy (KPFM) with elementary charge sensitivity at 300K. The NC active dopant concentration is measured as $N_D = 8.10^{20}$ cm^{-3} and $N_A > 5.10^{20}$ cm^{-3} for n- and p-type doping, respectively. The electrostatic equilibrium between the NC and the HOPG reference substrate is investigated, and reveals an enhancement of the Fermi level mismatch between the NCs and the HOPG substrate at reduced NC sizes, both for n- and p-type doping. It also shows, for n-type doped NCs with smallest sizes (~2 nm), the existence of a full depletion regime, in which smallest NCs contain single ionized dopants. Results are compared with self-consistent tight-binding calculations of the electronic structure of InAs NCs including hydrogenoid impurities and the presence of a host substrate, in the case of n-type doped NCs. The observed enhancement of the NC-HOPG Fermi-level mismatch can be understood by considering a size-dependent electrostatic contribution attributed to dipolar effects at the NC-ligand interface. The estimated surface dipole density equals a few Debye/nm², and is increased at smallest NC sizes, which follows the enhancement of ligand densities at small NC sizes previously reported for metallic or semiconducting NCs. The results put forward the role played by the NC-ligand interface electrostatics for electronic applications.

INTRODUCTION

Doped semiconductor nanocrystals (NCs)[1,2] are the subject of intensive research due to their potential applications in electronics or optoelectronics. They enable *e.g.* to fabricate semiconductor nanomaterials incorporating magnetic impurities[1], to synthesize nanostructures for photovoltaic applications[3], or to design plasmonic nanomaterials due to the large achievable doping concentration up to a few percent[4-8]. The synthesis of doped NCs is now available for a variety of materials. It includes non-colloidal NCs grown by physical methods such as Indium Tin Oxide[4], ZnO[5], or Si[6-8], but also NCs grown by colloidal chemistry such as CdSe[9], ZnS[10], or InAs[11,12]. The large concentration of impurities required to dope individual NCs with a few nm size has nonetheless raised fundamental questions such as the dopant solubility and the NC self-purification[13]. The control of doping processes as well as the structural and electrical characterization of dopants in NCs are still open fields of investigation[13-16].

In this Article, we focus on colloidal InAs NCs doped by diffusion[11]. This system offers a unique test bench to study electronic doping issues in colloidal systems, since both n-type (Cu) doping and p-type (Ag) doping can be achieved for InAs NCs, as qualitatively evidenced from optical and scanning tunneling spectroscopy (STS) experiments[11]. n-type and p-type dopings are however different in their essence, since Cu behaves as an interstitial dopant with high solubility in InAs[15], while Ag incorporates as a substituent of In with a finite low solubility limit, as evidenced from a recent structural work[16]. A strong need exists to characterize the active electronic doping of such colloidal NCs beyond structural considerations, and beyond early optical or STS experiments. This includes the accurate assessment of the NC active electronic doping level, which is of primary interest for electronic applications. It also includes the understanding of the electronic structure of

doped NCs, which may be strongly affected by the presence of dopants[11], and is insufficiently understood in link with experiments.

We investigate for this purpose in this Article n-type (Cu-doped) and p-type (Ag-doped) colloidal individual InAs NCs as a function of their size, in the ~2-8 nm size range. To characterize the NC doping, we use Kelvin Probe Force Microscopy (KPFM) experiments in ultra-high vacuum, enabling the measurement of the charge transfer between doped NCs and a highly oriented pyrolytic graphite (HOPG) reference substrate, with a charge sensitivity better than a single elementary charge, at room temperature. We observe for Cu-doped InAs NCs of different sizes a transition from a partial ionization regime towards a full depletion regime at smallest NC sizes. The ionization charge of fully depleted NCs is solely limited by the number of electrically active dopants, which enables to measure the NC active doping level (active donor and acceptor concentrations N_D and N_A) at $N_D=8.10^{20}$ cm^{-3} and $N_A > 5.10^{20}$ cm^{-3} for Cu or Ag doping, respectively. The combined KPFM characterization of n-type and p-type doped NCs also provides a spectroscopy of the Fermi level mismatch between the NC and the reference HOPG substrate, as a function of the NC size and doping type, which is not achievable by other techniques. The analysis reveals an enhancement of the NC-HOPG Fermi level mismatch at reduced NC sizes, which is compared to self-consistent tight-binding calculations of the InAs NC electronic structure including hydrogenoid impurities and substrate, in the case of n-type doped NCs. These results are only understood provided a size-dependent electrostatic contribution be introduced, which is attributed to dipolar effects at the NC-ligand interface. The estimated surface dipole density equals ~0.2 C/m, and is increased by a factor of ~3-4 at the smallest NC sizes, which corresponds to the enhancement of ligand densities at small NC sizes previously reported for metallic or semiconducting NCs. These results put forward the important role played by the electrostatics at the NC-ligand interface, in combination with doping.

METHODS

Nanocrystal synthesis. The detailed NC synthesis can be found in previous work[11,15]. Pre-synthesized colloidal InAs NCs with dodecylamine / didodecyl-dimethylammonium bromide (DDA/DDAB) ligands have been doped by diffusion of metal impurities at room temperature using a toluene solution containing metal salts ($CuCl_2$ and $AgNO_3$). Cu doping was used for n-type doping[11] with a Cu concentration of about 1500 Cu atoms / NC in solution during the doping procedure for a 5 nm size NC. The number of Cu atoms incorporated in NCs has been estimated from inductively coupled plasma atomic emission spectroscopy[15] and corresponds to about 465 Cu atoms / NC for a 5 nm diameter NC. Ag has been used for p-type doping, with a concentration of about 1660 Ag atoms / NC in solution for a 5 nm NC size, corresponding to about 170 Ag atoms / NC, however present both as dopants or clusters at the NC surface due to the finite solubility of Ag in InAs[16].

Sample preparation. Doped NCs dispersed in toluene have been stored under nitrogen in an oxygen-free (<1 ppm) environment. NCs have been deposited by drop casting from diluted toluene NC dispersions onto freshly cleaved highly-oriented pyrolytic graphite (HOPG) substrates (SPI Supplies) and transferred within a few minutes in a sealed container to the load-locks of the ultra-high vacuum atomic force microscopes used in this work (VT AFM/STM, Scienta Omicron, or JT AFM/STM, SPECS). Both set-ups have a base pressure in the 10^{-10} mbar range. We took a special care in experiments to obtain a clear phase separation between the bare HOPG substrate (used as a reference for Kelvin probe measurements[17]) and the excess ligand layer deposited together with the NCs. This was achieved by a mild sample temperature annealing in ultra-high vacuum (UHV) (T<140°C for 15 min) as illustrated in the Supporting Information (Figure S1 and S2).

Atomic force microscopy. Two atomic force microscopy set-ups were used in this work. The main set-up is an optical-beam AFM (VT AFM/STM, Scienta Omicron) using conventional metal-plated cantilevers (EFM PPP, Nanosensors) with resonance frequency f_0 of about 70 kHz and spring constant in the 1-3 N/m range. The oscillation amplitude of the cantilever (typical peak-to-peak oscillation amplitude A_{pp}=20 nm) has been carefully calibrated using the technique derived from the work of F. Giessibl[18]. The minimum distance between the lowest turning point of the tip oscillation and the substrate critically depends on the cantilever frequency shift detuning Δf. We used here mostly low frequency detunings (Δf=-5 Hz, corresponding to minimum tip-substrate distances in the 4-5nm range) to record simultaneous Kelvin probe and nc-AFM images while avoiding any role of short-range forces in Kelvin probe data used in a subsequent quantitative analysis. The role of Δf on nc-AFM topography images (in particular, on the measurement of a "true" NC height) is discussed in the core of our manuscript. This issue has been addressed by using a stiff-probe atomic force microscope (JT AFM/STM, SPECS) operating at low temperatures (in this work, T=77K). This set-up is based on a length-extensional quartz resonator (see e.g. Ref.[19] for high-resolution imaging on Silicon) with stiffness of about 5.10^5 N/m and oscillation amplitude A_{pp}=400pm. The sensors were used with a positive frequency shift detuning (Δf=+1Hz) to intentionally obtain nc-AFM topography images with significant repulsive force gradients (short range) contributions, for sake of comparison with optical-beam AFM topography images.

Kelvin probe force microscopy. Kelvin probe images have been recorded from the optical beam AFM (VT AFM/STM, Scienta Omicron) using Frequency Modulation (FM) KPFM or Amplitude Modulation (AM) KPFM. The two techniques differ since FM-KPFM (resp. AM-KPFM) is sensitive to electrical force gradients (resp. forces). Both techniques vary in their implementations, sensibilities, lateral resolutions and potential artifacts[20]. When measurements are conducted in the

regime of long-range electrostatic forces, both techniques can be analyzed quantitatively using conventional numerical electrostatic simulations[21-23]. FM-KPFM images are recorded by applying a low-frequency ac modulation (typically f_{mod} = 300Hz, V_{ac} = 200 mV) to the cantilever bias and compensating the ac cantilever frequency shift of the first flexural mode as a function of the tip dc potential. AM-KPFM images are recorded by electrically exciting the cantilever at its second flexural mode (typ. $f_{mod} = 6.2\ f_0$, V_{ac} = 200 mV) and nullifying the induced ac cantilever oscillation amplitude as a function of the tip dc potential.

Transmission Electron Microscopy. TEM measurements were performed using a Tecnai T12 G2 Spirit and Tecnai F20 G2. All size statistics are analyzed using the "Scion image" program.

Electrostatic numerical simulations. Numerical simulations enable to extract the actual electrostatic potential of individual ionized NCs from experimental KPFM signals, which suffer from averaging mechanisms due to stray capacitances and tip oscillation. Numerical simulations have been implemented using COMSOL as a Poisson solver according to the developments of Ref.[21] and can be obtained either in AM-KPFM[22] or FM-KPFM modes[23]. A dielectric description of the NCs is used for the simulations, considering the substrate as metallic and the NCs as an InAs semiconducting core (with relative dielectric constant ε_{InAs}=15.1) surrounded by a ligand shell considered as a dielectric material with $\varepsilon_{ligands}$=2.6. The thickness of the ligand layer is taken as 0.35 nm as from comparative AFM and TEM measurements. The result of the simulations is used, in practice, as a tool to transform raw experimental KPFM data into local electrostatic potentials, and to estimate the NC ionization charge assuming a charge distribution model (e.g. core charge or junction model)[24].

Tight binding numerical simulations. The electronic structure of pristine InAs NCs was calculated using a tight-binding approach in which each In or As atom is represented by 20 atomic orbitals

including spin degeneracy. We used the $sp^3d^5s^*$ model of Ref.[25]. The surface of the NCs is passivated by pseudo-hydrogen atoms. Doped NCs are described assuming that each dopant behaves as a hydrogenoid impurity characterized by a point charge $+e$ placed at an interstitial position plus an extra electron that fills the conduction states. The impurities are placed at random positions excluding surface sites. The total potential coming from the fixed charges and the electrons is added to tight-binding Hamiltonian[26]. The electronic states and the potential are solved self-consistently in a Hartree-like approach[27]. In the case of free-standing doped NCs, the Fermi level is determined by the number of electrons (impurities) occupying the conduction states. In the case of NCs in equilibrium with a metal (here HOPG), the Fermi level is imposed by the metal substrate and the number of electrons is considered as a variable that can take fractional values. In that case, the total potential also includes the effect of the metal substrate described using the image-charge method. The electronic states, the potential and the NC charge are obtained using a self-consistent iterative procedure.

RESULTS

To probe the charge transfers from the NCs to their environment, we use HOPG as a reference host substrate, since this material has a stable work function ($\chi_{HOPG} = 4.5$ eV[28]) almost insensitive to contamination in ambient air or vacuum[28]. The sample is prepared by NC drop casting from colloidal dispersions in anhydrous toluene[11] onto freshly cleaved HOPG. Samples are immediately loaded into ultra-high vacuum, followed by a mild sample annealing to improve the excess ligand layer ordering, if required. Non-Contact Atomic Force Microscopy (nc-AFM) and Kelvin Probe Force Microscopy (KFPM) experiments are then carried out (see Methods).

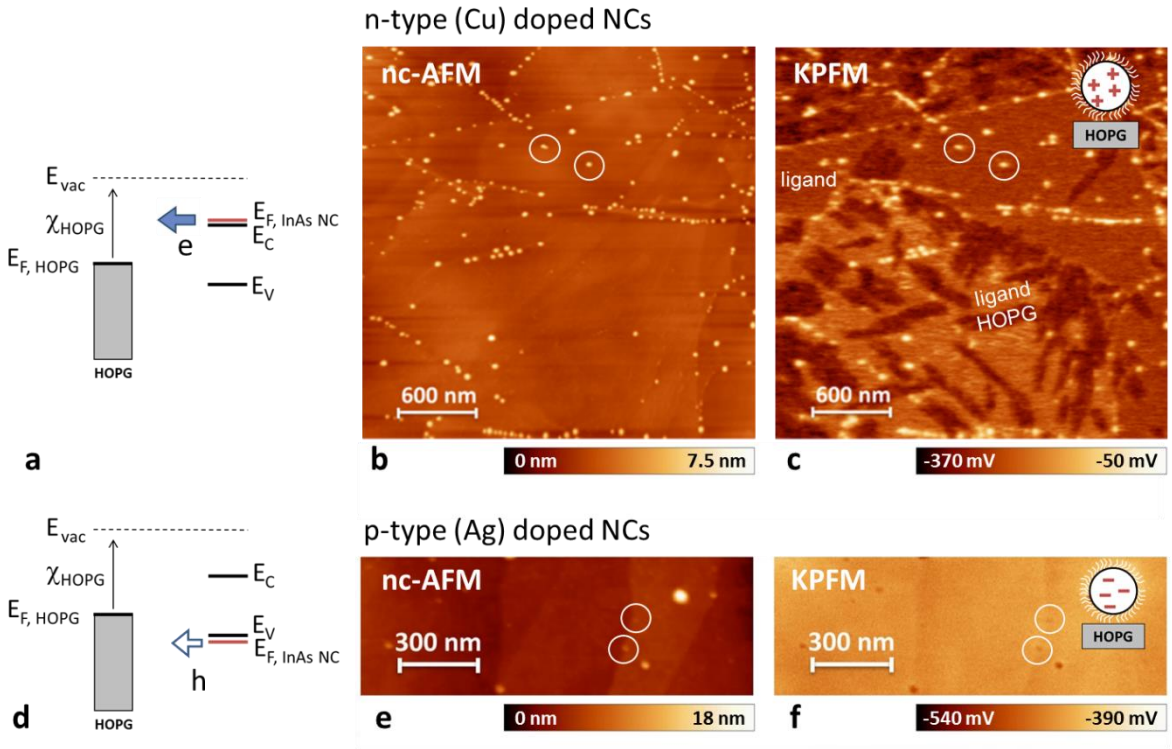

Figure 1: a) Energy diagram of HOPG (with work function χ_{HOPG}) and a highly n-type doped NC represented by its conduction and valence band ground levels E_c and E_v, and a Fermi level $E_{F,InAs\ NC}$ (we choose $E_{F,InAs\ NC}>E_C$ for simplicity). The vacuum level is E_{vac}. The arrow indicates the NC ionization process, in which the NCs become partially depleted and free electrons are transferred to HOPG, leaving the NC positively charged. b) nc-AFM image of Cu-doped NCs on HOPG, recorded with a cantilever with resonance frequency f_0~70 kHz, stiffness k~3N/m, and with a frequency shift detuning setpoint Δf=-5Hz and a peak-to-peak oscillation amplitude A_{pp}=20 nm. c) Simultaneously recorded frequency modulation KPFM image (electrostatic modulation frequency f_{ac}=300 Hz and amplitude V_{ac}=200 mV). The regulated KPFM dc bias is applied at the tip. Bright features correspond to positively charged NCs. d) Similar diagram as in a) for p-doped NCs. e) and f) nc-AFM and amplitude modulation KPFM images. Individual NCs are highlighted (the brighter features in the nc-AFM image correspond to agglomerated NCs). Dark features in the KPFM image correspond to negatively charged NCs. Scanning conditions are identical to b) and c) except for the use of an amplitude-modulation KPFM mode (modulation frequency $f_{ac} \sim 6.2\ f_0 \sim 420$ kHz).

Qualitative evidence for n- and p-type doping in KPFM experiments. The expected charge transfers from doped NCs are illustrated in Figure 1 in the case of n-type (Cu) and p-type (Ag) doped NCs. The Fermi levels for doped NCs in the inset of Figure 1 are placed for sake of simplicity beyond the conduction and valence band onsets as expected for degenerately doped bulk materials–this point will be specifically discussed hereafter based on tight-binding calculations. Assuming that the HOPG Fermi level falls within the NC band-gap before charge transfer, NC dopants are expected to ionize and transfer free electrons (resp. holes) towards the HOPG substrate (arrows in Figure 1 a and d) for n-type (resp. p-type) doping. This process leaves the NCs partially depleted, which corresponds to a positive (resp. negative) charging for the n-doped (resp. p-doped) NCs on the HOPG substrate. This picture qualitatively matches with KPFM experiments shown in Figure 1. KPFM images here correspond to maps of the sample electrostatic potential, since we chose to apply the regulated dc compensation bias to the AFM tip (see Methods). KPFM images of doped NCs are shown in Figure 1c and f, for n-type and p-type doped NCs, respectively. They exhibit bright features (positive NC charging) and dark features (negative NC charging), respectively. This observation agrees with the energy diagrams in Figure 1a and d. Such a charge transfer mechanism has been observed experimentally for n-doped hydrogen-passivated Si NCs[21]. Both n- and p-type NC doping have however not been observed for Si NCs due to difficulties in reaching an effective doping for p-type NCs[21,24]. Additional features observed in the KPFM image in Figure 1c correspond to the presence of an excess sub-monolayer of ligands on the HOPG substrate (Figures S1 and S2).

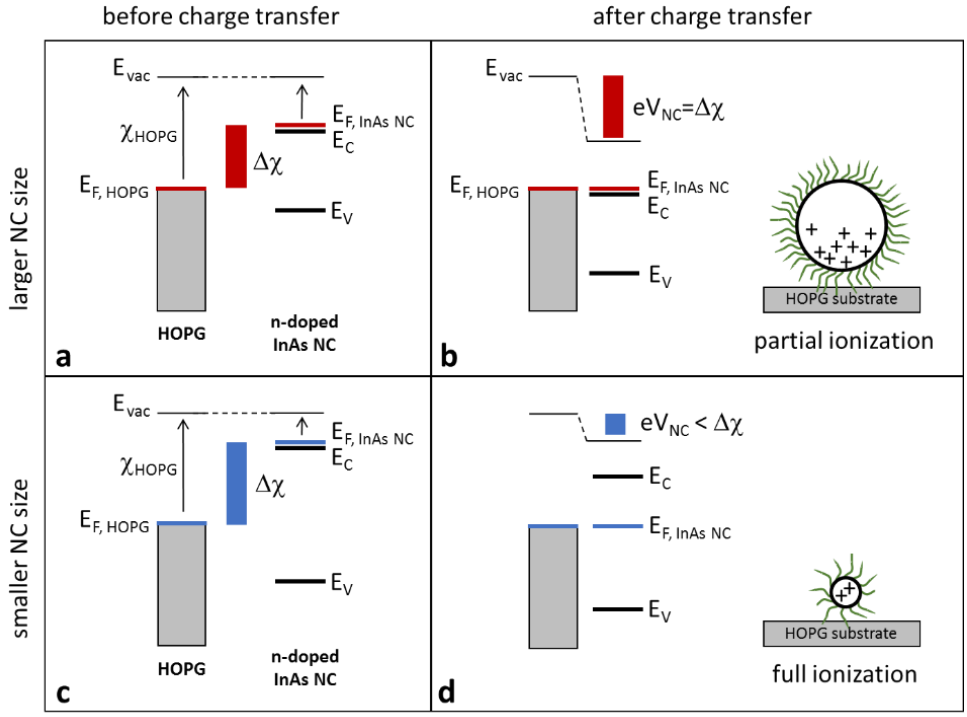

Figure 2: a) Energy diagram of HOPG (with work function χ_{HOPG}) and a n-type doped NC with conduction and valence band ground levels E_c and E_v, and Fermi level $E_{F,InAs\ NC}$ (choosing $E_{F,InAs\ NC} > E_c$). b) Energy diagram at equilibrium after charge transfer in the partial ionization (depletion) limit. The NC electrostatic potential V_{NC} compensates for the Fermi level mismatch $\Delta\chi = E_{F,InAs\ NC} - E_{F,HOPG}$ (in red) prior to charge transfer. A depleted junction forms at the NC/HOPG interface (see text). c) Same energy diagram as in a) but for a NC with smaller size and containing only a few dopants. An enhancement of the Fermi level mismatch $\Delta\chi = E_{F,InAs\ NC} - E_{F,HOPG}$ is introduced, assuming in a simple picture an increase of the NC band-gap upon quantum confinement (see text for a discussion). d) Energy diagram after charge transfer drawn in the full ionization (depletion) limit, in which the NC electrostatic energy eV_{NC} (in blue) cannot reach and equilibrate the mismatch $\Delta\chi$, due to an insufficient number of dopants in the NC.

Partial and full ionization (depletion) regimes. We now focus on the charge state of ionized NCs. Energy diagrams drawn before and after charge transfer are described in Figure 2 in the case of n-doped NCs. Similar diagrams would apply for p-doped NCs, but are not represented. As depicted in Figure 2a and 2b, when the NCs contain enough dopants to account for $\Delta\chi = E_{F,InAs\ NC} - E_{F,\ HOPG}$,

which is the relevant case for large size NCs, an electrostatic equilibrium sets in and compensates for the Fermi level mismatch prior to charge transfer between the doped NCs and the HOPG substrate[21,24] ($\Delta\chi$ is shown as a red bar in Figure 2a and b). In this situation, the NCs become only *partially* ionized, and a depletion layer (junction) builds in at the interface with the substrate, as previously analyzed in the case of n-doped Silicon NCs[24]. A second scenario may occur if the NCs do not contain enough active dopants to ensure an electrostatic compensation of the Fermi level mismatch $\Delta\chi$ upon charge transfer. This situation leads to a full NC ionization (or depletion) regime, in which the NC ionization charge equals the number of electrically active dopants in the NCs. However, the NC electrostatic energy eV_{NC} remains less than $\Delta\chi$ (see Figure 2 c and d). The occurrence of such a scenario strongly depends on the NC size range (including quantum confinement issues) and doping (including band tailing or filling issues). It will be discussed later by comparison with self-consistent tight-binding calculations for doped NCs. The NC size required to observe a full depletion regime can nonetheless be roughly estimated by noticing that for NCs with a few nm size, both $\Delta\chi$ and the electrostatic confinement energy of a NC carrying an elementary charge fall in the eV range[21,24,29]. Thus, the full ionization scenario of Figure 2c and d is expected for NCs containing single (or at most a few) active dopants. It corresponds to NCs with sizes of a few nm, assuming a doping level in the 10^{20} cm^{-3} range. A crossover between the partial ionization and the full depletion regimes as a function of the NC size has not been observed experimentally in literature so far. Its signature would be here a reduction of the NC electrostatic energy eV_{NC} (see Figure 2b and 2d) in the full depletion regime, due to the limitation of eV_{NC} by the number of available dopants. The observation of such a transition (see below) also provides a method to measure the concentration of electrically active dopants in NCs, since the NC depletion charge exactly equals the number of electrically active dopants in the full depletion regime.

Quantitative analysis of the KPFM data. We performed a quantitative analysis of the NC charge state and electrostatic potentials based on combined nc-AFM and KPFM measurements. The analysis is carried out both for n-type (Cu) and p-type (Ag) doped NCs, as well as for intrinsic reference NCs (see Supporting Information), as a function of their size in the 2-8 nm size range, taking advantage of the nominal dispersion of the NC sizes as from NC solutions with average size of about 4-5 nm. Working beyond qualitative imaging requires extra experimental care to achieve a quantitative analysis of doping concentrations. One step consists in recording KPFM signals of individual NCs in the long-range electrostatic force field, in order to ensure a convenient quantitative analysis using a long-range electrostatics formalism[22]. Such a method has already been applied to the case of Si NCs[21], or to nanoscale domains in organic donor acceptor photovoltaic blends[23]. Quantifying the doping concentration additionally requires measuring the NC size accurately, which is critical to determine the volume of small-size NCs. A drawback of using atomic force microscopy stems however from the fact that the recorded NC heights may not be correct in the long-range force regime. Such an issue has been reported for tapping mode imaging of NCs[30]. It was addressed in a more recent study using combined nc-AFM and KPFM on molecular layers[31], demonstrating that correct height measurements can be recovered using this combined powerful approach (see Supporting Information Figure S3), while working with large frequency shift topography set-points in the short-range (dissipative) regime.

Procedure for NC size and KPFM measurements. We worked here according to the conclusions of Ref.[31]. KPFM images have been recorded in the long-range force regime using a small cantilever frequency shift detuning Δf=-5 Hz (measured NC average height $\langle h \rangle = 4.5 \pm 0.1$ nm, see Figure S4). The NC correct heights have been recorded by using a larger frequency shift detuning Δf=-18 Hz in the dissipative regime (measured NC height distribution $\langle h \rangle = 5.13 \pm 0.1$ nm, see Figure S4 and Figure SI for a NC per NC comparison). We separately measured the NC height distribution

using a stiff-probe AFM (SPECS JT AFM/STM) operated with a positive frequency detuning to ensure the use of repulsive short-range forces. The corresponding height statistics provides an average NC height <h>= 5.2 ± 0.2 nm (see Figure S4). The error bar on the average height is due to the finite number of investigated NCs (here, 55 NCs imaged at low temperature). The measured distribution falls in agreement with data obtained at large Δf (<h>= 5.13 ± 0.1 nm), but offset by Δh= 0.7 ± 0.1 nm with respect to imaging at Δf=-5 Hz (see Figure S4). This value of Δh was used to correct NC heights from nc-AFM images recorded at Δf=-5 Hz. Only corrected heights have been used in the following.

TEM imaging and estimation of the ligand layer thickness. We finally compared the NC height measurements to size measurements obtained from transmission electron microscopy (TEM) on n-type (Cu) doped NCs from the same batch (see Methods). A TEM micrograph and a size statistics are shown in Figure S4. The average NC size (diameter) measured from TEM is smaller in comparison with AFM measurements, and equals <d>=4.5 nm. This lower value is explained by the fact that TEM is not sensitive to the NCs ligand layer but only to the inorganic NC core. By comparison with nc-AFM data acquired in the dissipative regime (<h>=5.1 ± 0.1 nm for cantilever-based nc-AFM, and <h>=5.2 ± 0.2 nm for nc-AFM carried out with a stiff probe), we therefore estimate a ligand layer thickness of about 6 -8 Å. This value is smaller than the length of the individual ligand molecules in vacuum, which indicates the relaxation of ligands, as shown in previous work on semiconducting and metallic NCs[32,33].

Quantitative KPFM analysis of n-type (Cu) doped NCs. We now focus on the quantitative analysis of the doped NC KPFM signals, starting with n-type (Cu) doped NCs. Raw NC KPFM signals are plotted in Figure 3a as a function of the NC corrected height, and show a gradual decrease of KPFM signals with reduced NC sizes. This feature is a priori counterintuitive–an enhancement of

$\Delta\chi$ with the NC quantum confinement would rather be expected in the picture of Figure 1. A straightforward explanation however comes from side-capacitance effects known to take place in KPFM experiments[34], which lead to an averaging between the actual NC electrostatic potential and the substrate surface potential. The averaging process highly depends on the NC size, but also on the tip oscillation, as well as on the choice of the FM or AM KPFM imaging mode. KPFM signals can however be deconvoluted from side-capacitance effects using numerical simulations[22] (see Methods and Supporting Information Figure S6). Since the modelling is purely electrostatic, a NC dielectric description is used, based on measured values for the NC core and ligand thickness previously determined from nc-AFM and TEM experiments. A core charge model is used in order to describe the ionized dopants[22], in which an effective charge Q_{core} is located at the NC center. Such a model is effective, and meant to account for the surface dipole generated by the ionized NC on the substrate, and, in practice, to derive the ionized NC electrostatic potential V_{nc} from experimental data. The actual amount of charge carried by the NC will however depend on the actual ionized dopant distribution within the NC, which may form a depleted junction at the NC-substrate interface in the partial ionization regime[24]. The core charge model is however well adapted in the full depletion regime, even though the dipole generated by the NC ionized charge (and thus the corresponding KPFM signal) still depends on the exact charge location within the NC in the few dopant limit. Hence, the experimental KPFM signal of a NC carrying a single ionized dopant will be "viewed" in the core charge analysis as a NC with a core charge Q_{core} in the 0-2e range, depending on the dopant location, *i.e.* with the dopant located at the NC-substrate interface, or located at the NC top.

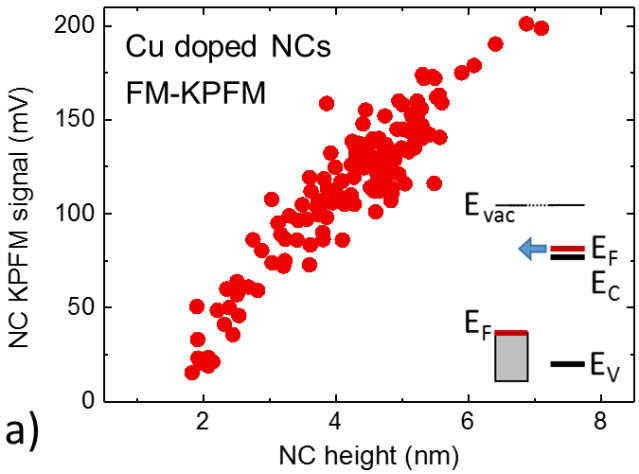
Cu doped NCs
FM-KPFM
NC KPFM signal (mV)
NC height (nm)
E vac
E F
E C
E F
E V
a)

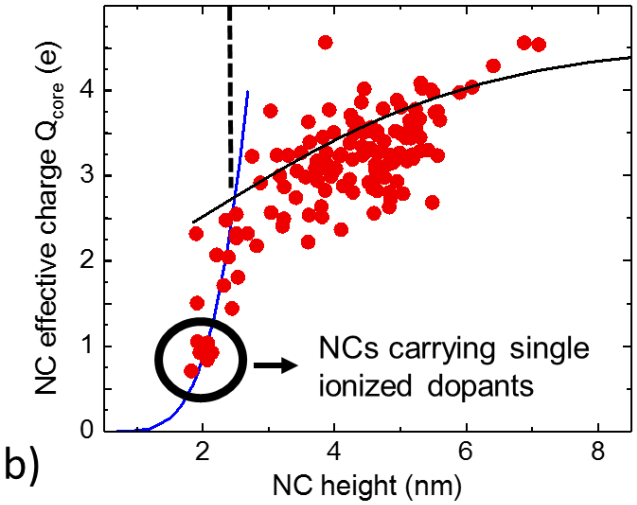
NC effective charge Q core (e)
NCs carrying single
ionized dopants
NC height (nm)
b)

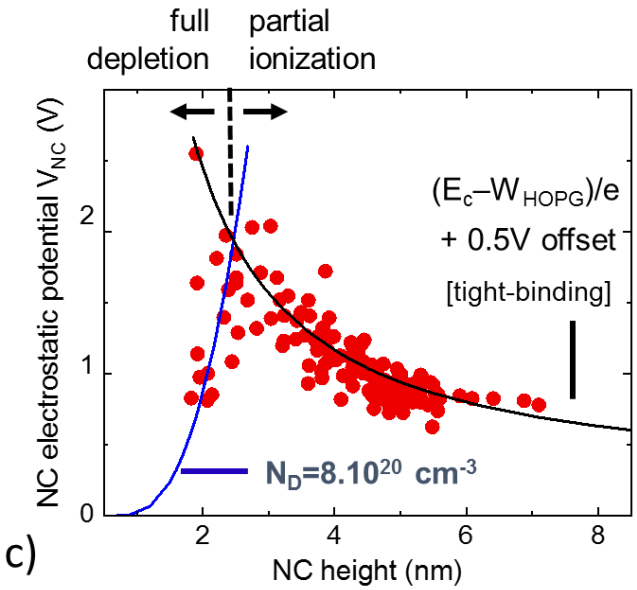
full
depletion
partial
ionization
NC electrostatic potential V NC (V)
(E c–W HOPG)/e
+ 0.5V offset
[tight-binding]
N D=8.10 20 cm -3
NC height (nm)
c)

Figure 3: a) FM-KPFM contrast of individual n-type (Cu) doped NCs plotted as a function of their corrected height. The inset shows the energy diagram prior to charge transfer. b) NC effective core charge calculated from a). The blue continuous line is a fit to data in the full depletion regime, leading to a doping concentration N_D=8.10^{20} cm^{-3} (see text). The black continuous line corresponds to the line fitted in c). The core charge values of smallest NCs (highlighted points) correspond to the single ionized dopant limit. c) NC electrostatic potential calculated from a). The black continuous line describes, as a guide to the eye, the evolution of the NC conduction band E_c with respect to the HOPG Fermi level for undoped NCs, with a phenomenological 0.5 eV offset (see text). The blue continuous lines corresponds to the line fitted in b). The sharp potential drop at small NC size is attributed to the crossover towards the full depletion.

The NC core charge Q_{core} and the electrostatic potential V_{NC} extracted from raw KPFM signals are shown in Figure 3b and 3c, respectively. No adjustable parameter was introduced in the analysis. The NC electrostatic potential is increased as the NC size is reduced (black continuous line in Figure 3c), which corresponds to an enhancement of the Femi-level mismatch between the doped NCs and the reference HOPG substrate. A first explanation stems from quantum confinement effects, which push towards higher energy the onset of the conduction band levels for undoped NCs. Assuming in a naïve view that the NC Fermi level follows the conduction band of the undoped NCs due to degenerate doping, this provides a tentative prediction of the Femi-level mismatch between the doped NCs and the reference HOPG substrate. This effect is represented by the black line in Figure 3c as a guide to the eye from the tight-binding calculation of undoped InAs NC conduction band levels[29], introducing an electrostatic potential offset of 0.5 eV. However, other effects such as band filling or tailing[11], or electrostatic effects at the NC-ligand interface have to be considered. They will be discussed in the following, based on tight-binding calculations for doped NCs, and will discard the simple quantum confinement picture taken at this stage.

A striking effect occurs additionally at smallest NC size (typically below 2 nm), with the observation of a sharp decrease in the NC electrostatic potential V_{NC}. We attribute this transition to the crossover between the partial ionization and full depletion regimes described in Figure 2. In the full depletion regime, the NC electrostatic potential V_{NC} is equal to the product of the NC average charge and of the electrostatic potential of a NC carrying an elementary charge (see Supporting Information Figure S6). We use this property to estimate the NC doping from a fit of the electrostatic data of Figure 3b and 3c at small NC size, taking as a rough approximation a continuous charge model as a function of the NC size. The values of V_{NC} at small NC size are well accounted for using an active dopant concentration $N_D \sim 8.10^{20}$ cm^{-3} (blue line in Figure 3b). The agreement is further supported by examining the NC effective core charge in Figure 3b. At small NC size, the NC core charge Q_{core} falls in the range 0-2e, as expected for NCs carrying single ionized dopants. In particular, for NC sizes around 2 nm, the Q_{core} values correspond to elementary charges (see highlighted points). The agreement is even more striking that no adjustable parameter has been used in the simulations. A comparative analysis of n-type (Cu) doped and (reference) intrinsic InAs NCs is additionally provided in Figure S7 in the Supporting Information.

Quantitative KPFM analysis of p-type (Ag) doped NCs. We now switch to the case of p-type (Ag) doped NCs. Care has to be taken because of the finite solubility limit of Ag in InAs. Ag atoms indeed incorporate as dopants at the NC surface in the so-called "doping regime", but also tend to form surface clusters in the "growth region" beyond the solubility limit[16]. The number of Ag dopants introduced in NCs in the doping regime also stays at most constant as a function of the NC size[16]. This would correspond to a strong reduction of the doping concentration N_A with increased NC size, but this effect is a priori "transparent" in KPFM experiments, provided the NCs contain enough dopants to ensure an equilibrium in the partial ionization regime, as in Figure 2a.

We applied to p-type (Ag) doped NCs the same analysis of experimental data as for n-type (Cu) doped NCs, however keeping in mind that an estimation of the NC doping level N_A should only be valid for NCs with smallest sizes, and not through the full NC size range. Experimental KPFM signals for p-type (Ag) doped NCs are shown in Figure 4a. Data have been here recorded in the amplitude modulation (AM) KPFM mode. The NC electrostatic potential is shown in Figure 4c, and has been derived from data from Figure 4a by taking into account an additional side capacitance effect associated with the cantilever itself in the AM-KPFM mode[22,34], (capacitance gradient of 2.4 10^{-11} F/m for the cantilevers used in this work, as determined from a numerical simulation). This contribution was included in the formalism of Ref.[22], in order to calculate the values of V_{NC} and Q_{core} from raw AM-KPFM data. As seen in Figure 4c, the NC electrostatic potential is enhanced while reducing the NC size. The values for the mismatch between the NC valence band E_V and the HOPG substrate Fermi level for undoped NCs are also shown as a guide to the eye (continuous black line) as derived from tight-binding calculations for undoped NCs[29]. This includes a phenomenological electrostatic offset of +0.5 V, as in the case of Cu-doped NCs. The main difference with n-type NCs is that no sharp decrease in the values of V_{NC} is observed at small NC size, indicating that the full depletion regime is not reached for p-type doped NCs. This point agrees with the values for the effective core charge Q_{core} shown (Figure 4b) which do not clearly fall in the [0-2e] range as for n-type doped NCs in Figure 3b. The apparent absence of a cross-over towards a full depletion regime for p-type (Ag) doped NCs may be due a larger acceptor density as compared to the n-type (Cu) doped NC samples, or potentially due to double acceptor configuration for Ag dopants in InAs, as originally put forward in substitutional doping scenario[11]. Only a minimum doping level $N_A > \sim 5.10^{20}$-10^{21} cm^{-3} can therefore be estimated from the KPFM analysis of Figure 4b.

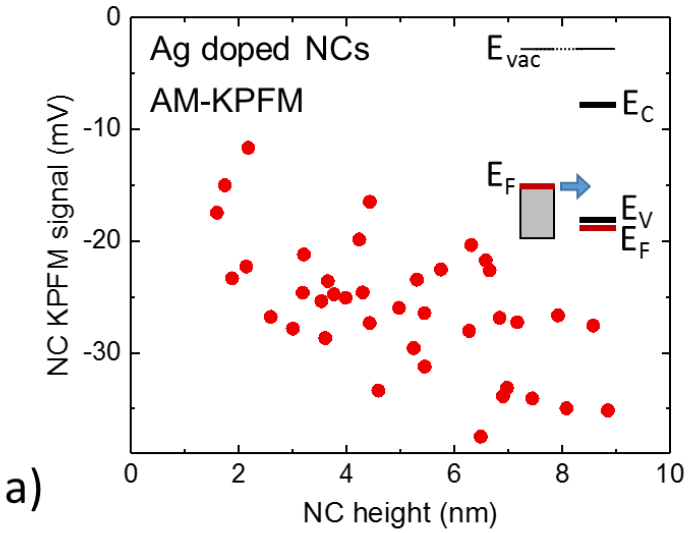
Ag doped NCs
AM-KPFM
E_{vac}
E_C
E_F
E_V
E_F
NC KPFM signal (mV)
0
-10
-20
-30
0
2
4
6
8
10
NC height (nm)

a)

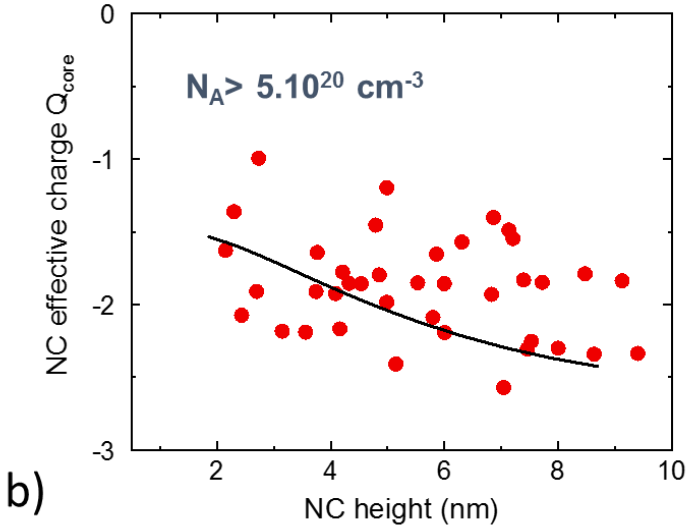
$N_A > 5.10^{20}$ cm^{-3}
NC effective charge Q_{core}
0
-1
-2
-3
2
4
6
8
10
NC height (nm)

b)

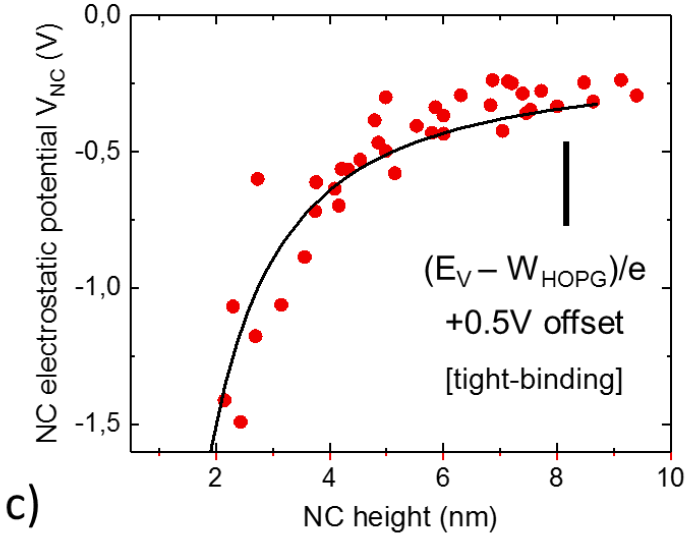
NC electrostatic potential V_{NC} (V)
0,0
-0,5
-1,0
-1,5
$(E_V - W_{HOPG})/e$
+0.5V offset
[tight-binding]
2
4
6
8
10
NC height (nm)

c)

Figure 4: a) Experimental AM-KPFM contrast of individual p-type (Ag) doped NCs plotted as a function of the NC corrected height. The inset schematics shows the energy diagram prior to charge transfer. b) NC effective core charge Q_{core} calculated from data plotted in a). The black continuous line corresponds to the model used in c). A dopant concentration $N_A>5.10^{20}$ cm^{-3} can be estimated from the ionization charge of NCs with smallest sizes (see text). c) NC electrostatic potential calculated from data shown in a). The black line describes the evolution of the NC valence band E_V with respect to the HOPG Fermi level upon quantum confinement for undoped NCs (see text). A phenomenological 0.5 eV offset is introduced as in Figure 3.

Comparison with tight-binding calculations of n-type doped NCs. We now focus on the comparison between experimental results and tight-binding calculations of doped InAs NCs. p-type (Ag) doped NCs are discarded from the analysis due to their specific structural doping issues (surface doping and dopant clustering)[16]. We only deal with n-type (Cu) doped InAs NCs, for which interstitial hydrogenoid dopants randomly distributed in the NC volume are considered (see Methods). The effect of dopants on the electronic structure of InAs NCs is illustrated in Figure 5a and b for an InAs NC with an InAs core effective diameter of about 2.4 nm either undoped (Figure 5a), or doped with four dopants (Figure 5b, dopant concentration N_D~6.10^{20} cm^{-3}). The reference for energies in Figure 5a and b corresponds to the valence band of bulk InAs. As described in Ref.[11], the introduction of dopants generates electronic states below the conduction levels of undoped NCs, *i.e.* band tailing, this effect being balanced by the population of the conduction electronic states, *i.e.* band-filling. Here, due to spin degeneracy, two electronic levels are populated while four NC dopants have been introduced. The NC Fermi-level is indicated in red in Figure 5b. It has an energy close to – but below – the first conduction level of the undoped NC in Figure 5a. This observation already breaks the simple picture used in the simplified energy diagrams of Figure 1 and Figure 2, although the donor concentration (here, N_D~6.10^{20} cm^{-3}) is by far beyond the degenerate limit for bulk InAs, of conduction band effective density of states $N_C<10^{17}$ cm^{-3}.

Another change in the electronic structure stems from the ionization process when the NCs are not considered in vacuum (as in Figure 5a and b), but rather brought in contact with an electron reservoir, as experimentally achieved in KPFM experiments. Removing an electron from a NC in a charge transfer process indeed changes the NC energy level filling, but it also introduces an additional electrostatic potential energy, which alters in return the NC electronic level structure. In order to describe this issue, the tight-binding calculations for doped NCs have been inserted in a self-consistent calculation ensuring the NC equilibrium with a metal substrate positioned 3.5 Å below the NC (this distance corresponds to the effective ligand thickness as determined from experiments). In this process, a NC gets ionized until its Fermi level equilibrates with the substrate reference Fermi level. The electronic structure of the doped NC used in Figure 5b is shown in Figure 5c, when brought in equilibrium with the substrate (an electrostatic offset of +0.75 eV has been introduced here). The energy reference in Figure 5c is the Fermi level of the metal substrate. In this example, the ionization charge carried by the NC is ~+ 2e, as illustrated by the Fermi level which accounts for the filling of only one NC conduction level, as compared to the two populated levels in Figure 5b prior to charge transfer. The change in the NC electronic structure upon charge transfer is also visible, for instance from the energies of the first confined conduction band levels, or from the NC apparent band-gap. This point attests to the need for a self-consistent approach to calculate the electronic structure of doped NCs for the interpretation of KPFM experiments.

We show in Figure 5 the results of the self-consistent tight binding calculations for the NC electrostatic potential (Figure 5d) and for the NC ionization charge (Figure 5e). Expected charge transfers are first predicted using nominal parameters for the electronic structure of InAs nanocrystals (using a 4.9 eV affinity value for bulk InAs) in equilibrium with the HOPG substrate (with work function $\chi_{HOPG} = 4.5$ eV).

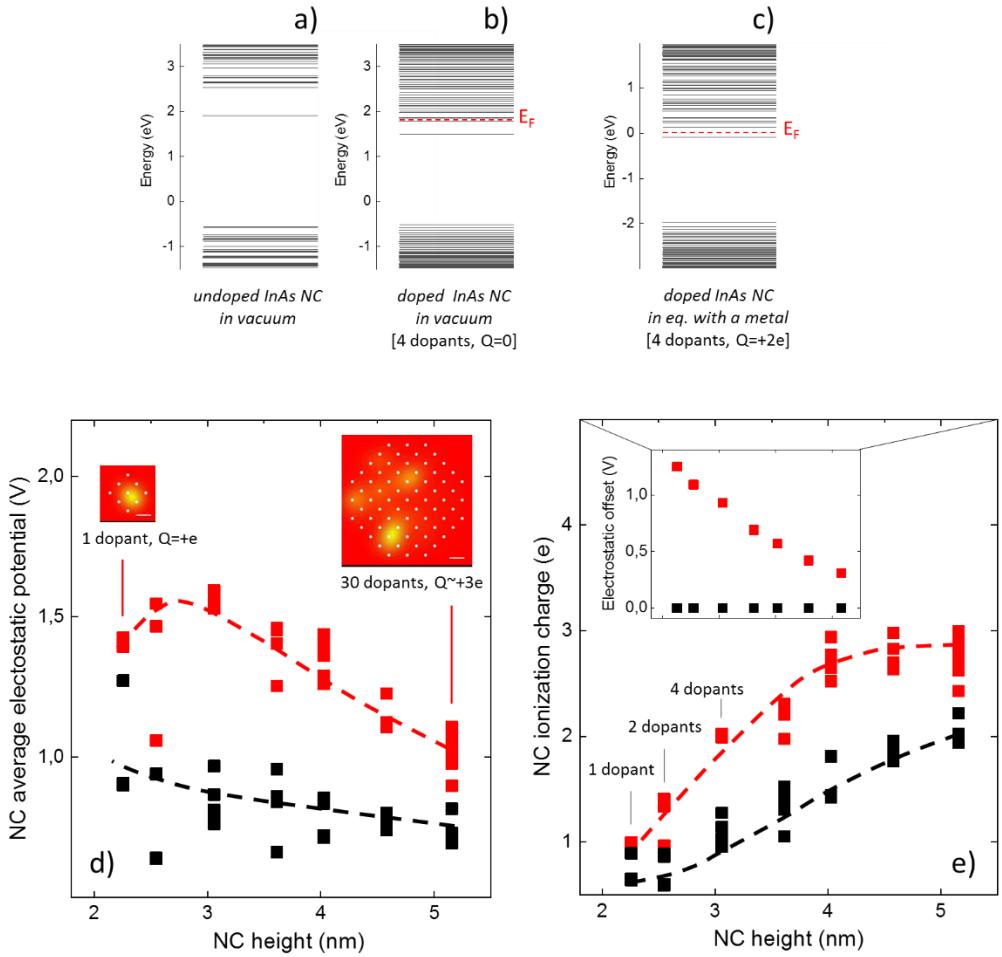

Figure 5: Tight-binding calculation of the electronic levels of an InAs NC with core diameter of about 2.4 nm (NC height of about 3.1 nm, including ligands) either a) undoped or b) doped with four hydrogenoid dopants (N_D=6. 10^{20} cm^{-3}). The reference for energies in a) and b) is the onset of the valence band of bulk InAs. c) Same calculation as in b) except that the NC is brought in equilibrium with a metal substrate (taken here as a reference for energies), and the NC electronic structure is calculated self-consistently. Here, the NC carries an ionization charge of ~+2e (two electrons have been transferred to the metal substrate). The Fermi levels are indicated in b) and c) by a dashed red line. d) Calculated NC electrostatic potential and e) calculated NC ionization charge plotted as a function of the NC height. Black points refer to nominal self-consistent tight binding calculations, while red points additionally include the electrostatic offset shown in the inset of e) (see text). The inset in d) corresponds to cross sections of the ionized NC electrostatic potential maps for two NCs.

Calculation results (black points in Figure 5d and 5e) reveal weaker charge transfers than experimentally observed. This is obvious (i) from the values of the average NC electrostatic potential, which are much weaker in Figure 5d (black points) than values shown in Figure 3c; and (ii) from the fact that the full depletion regime is *not* reached for NCs with smaller sizes in Figure 5e (black points), as compared with the experimental results shown in Figure 3b. Charge transfers therefore appear to be experimentally higher than theoretical predictions. To account for this, we introduce in the calculations an electrostatic contribution to the NC electrostatic potential as a phenomenological supplementary parameter. This contribution is introduced as a rigid shift of the NC energy levels prior to the self-consistent procedure. It is equivalent in its principle to the +0.5 V electrostatic offset used in the analysis of the electrostatic potential of ionized NCs in Figure 3 and 4, except that the offset is now introduced in the self-consistent tight-binding calculations developed for *doped* NCs. We speculate that the offset originates in the electrostatics of the NC-ligand interface, which has been discarded so far in our analysis. This hypothesis agrees with the fact that excess ligands deposited on the HOPG surface exhibit electrostatic features in KPFM images (Figure 1c), which is consistent with a dipolar character. Assuming an interface dipole of magnitude ~1 Debye per ligand, a 0.5 V electrostatic offset is reached for a surface ligand density of a few nm^{-2}, which is a typical value for ligand densities[33, 35, 36]. This corresponds to a dipole density of ~0.2 C/m (here, with dipoles oriented towards the outside of the NCs). We show in Figure 5d and Figure 5e the results of self-consistent tight-binding calculations for doped InAs NCs, introducing the size dependent electrostatic offset shown in the inset of Figure 5e (red points). The offset has been chosen to reproduce the experimental enhancement of the NC electrostatic potential with reduced NC sizes observed in Figure 3b. An illustration of the NC ionized dopant distribution is shown in the inset of Figure 5d for two NCs, revealing the distribution of ionized dopants in the NCs. The NC average electrostatic potential derived from the self-consistent tight-

binding calculations is shown in Figure 5d (red points) and now reproduces data of Figure 3b, when taking into account the electrostatic offset. It exhibits, as in Figure 3c, a drop at smallest NC size, which suggests that a full ionization regime is achieved, as in Figure 3. This is confirmed by the plot of the NC ionization charge shown in Figure 5e (red points), showing that smallest NCs - which carry single dopants - also carry a +1e ionization charge, and are thus in the full ionization limit. The introduction of a size-dependent electrostatic offset therefore enables a full agreement with the experimental data. Its dependence on the NC size can be attributed to the increase of the ligand surface densities at small NC size. This effect has already been put forward in the case of gold NCs[35] and more recently in the case of semiconductor NCs[36] and originates in a favored steric configuration and/or enhanced defect ratios at small NC radii. Such an enhancement reaches a factor 3 for Au NCs[35] in a size range similar to our work. This enhancement of ligand densities agrees with the values for the electrostatic potential offset introduced in the calculations and shown in Figure 5e (inset), ranging from ~ 0.3V at large NC size, and reaching ~ 1 V for the smallest NC size. Our analysis therefore highlights the impact of the electrostatic properties of the ligands onto the electronic properties of doped NCs, an effect which has not been studied in detail thus far.

CONCLUSION

In conclusion, we have investigated the doping properties of n- and p-type InAs colloidal nanocrystals from KPFM experiments operated in ultra-high vacuum with single charge sensitivity at room temperature. The analysis of charge transfers from doped NCs to the HOPG substrate has been carefully achieved in the 2-8 nm size range. We have shown evidence of a full ionization regime for the smallest NCs in the case of n-type doped NCs and measured the NC active dopant concentration (here, $N_D = 8.10^{20}$ cm^{-3} and $N_A > 5.10^{20}$ cm^{-3} for n- and p-type doping, respectively).

A self-consistent tight-binding analysis of the InAs NC electronic structure has been proposed and compared with experiments. It shows that an electrostatic contribution is required in order to match with experimental data, which we attribute to dipolar effects at the NC-ligand interface. The estimated surface dipole density equals a few Debye/nm^2 (with a dipole oriented toward the outside of the NCs). This dipolar effect increases at small NC sizes, which follows the enhancement of ligand densities at small NC sizes reported for metallic or semiconducting NCs. Our results put forward the role played by the NC-ligand interface with respect to electronic applications.

AUTHOR INFORMATION

Corresponding Author

thierry.melin@iemn.fr

Author Contributions

The manuscript was written through contributions of all authors. All authors have given approval to the final version of the manuscript.

SUPPORTING INFORMATION

Figure S1: Excess ligand layer ordering upon sample annealing.

Figure S2: Nanocrystal KPFM signals before and after thermal annealing.

Figure S3: nc-AFM sample topography with and without KPFM signal regulation.

Figure S4: Comparative NC size distributions in optical-beam / stiff-probe AFM and TEM.

Figure S5: Relationship between the NC heights measured at small and large frequency shift detuning Δf.

Figure S6: Calculated electrostatic potential V_{NC} and KPFM signals V_{KPFM} for a NC carrying a single charge.

Figure S7: Undoped InAs NC analysis

ACKNOWLEDGMENT

This work has been performed by using the facilities of the French RENATECH network and of the ExCELSiOR Nanoscience Characterization Center at IEMN. We thank H. Diesinger for support with Kelvin probe microscopy experiments, and D. Guérin for fruitful discussions, and A. Dufrêne for illustrations. We acknowledge financial support from the French National Research Agency under contracts ANR-11-BS10-000, ANR-15-CE09-0004-04 and ANR-13-BS09-0020.

ABBREVIATIONS

NC, nanocrystal; AFM, atomic force microscopy; DDA/DCAB, dedecylamine / didodecyl-dimethylammonium; HOPG, highly-oriented pyrolytic graphite; UHV, ultra-high vacuum ; AM, amplitude modulation; FM, frequency modulation; nc-AFM, non-contact AFM; KPFM, Kelvin Probe Force Microscopy; TEM, Transmission Electron Microscopy; STS, scanning tunneling spectroscopy.

REFERENCES

(1) *see e.g.* Norris, D.J.; Efros, A.L.; Erwin, S.C. Doped Nanocrystals, *Science* **2008,** *319,* 1776.

(2) *for a recent review, see* Pradhan, N.; Adhikari, S. D., Nag, A., Sarma, D. D. Luminescence, Plasmonic, and Magnetic Properties of Doped Semiconductor Nanocrystals, *Angew. Chem. Int. Ed.* **2017,** *56,* 7038 –7054.

(3) Gur, I., Fromer, N. A.; Geier, M. L.; Alivisatos, A. P. Air-Stable All-Inorganic Nanocrystal Solar Cells Processed from Solution, *Science* **2005,** *310,* 462.

(4) Wang, T.; Radovanovic, P.V. Free Electron Concentration in Colloidal Indium Tin Oxide Nanocrystals Determined by Their Size and Structure, *J. Phys. Chem. C* **2011,** *115,* 406–413.

(5) Buonsanti, R. ; Llordes, A.; Aloni, S.; Helms, B. A.; Milliron, D. J. Tunable Infrared Absorption and Visible Transparency of Colloidal Aluminum-Doped Zinc Oxide Nanocrystals, *Nano Lett.* **2011,** *11,* 4706–4710.

(6) Rowe, D. J.; Jeong, J. S.; hoyan, K. A.; Kortshagen, U. R. Phosphorus-Doped Silicon Nanocrystals Exhibiting Mid-Infrared Localized Surface Plasmon Resonance, *Nano Lett.* **2013**, *13,* 1317–133.

(7) Zhang, H. ; Zhang, R. ; Schramke, K. S. ; Bedford, N. M. ; Hunter, K. ; Kortshagen, U. R. ; Nordlander, P. Doped Silicon Nanocrystal Plasmonics *ACS Photonics* **2017,** *4,* 963–970.

(8) Pi, X.; Delerue, C. Tight-Binding Calculations of the Optical Response of Optimally P- Doped Si Nanocrystals: A Model for Localized Surface Plasmon Resonance. *Phys. Rev. Lett.* **2013,** *111,* 1–5.

(9) *see e.g.* Erwin, S. C.; Zu, L.; Haftel, M. I.; Efros, A. L.; Kennedy, T. A.; Norris, D. J. Doping Semiconductor Nanocrystals, *Nature* **2005,** *436,* 91-94.

(10) Bhargava, R. N.; Gallagher, D.; Hong, X.; Nurmikko, A. Optical properties of manganese-doped nanocrystals of ZnS. *Phys. Rev. Lett.* **1994,** *72*, 416.

(11) Mocatta, D.; Cohen, G.; Schattner, J.; Millo O.; Rabani, E.; Banin, U. Heavily Doped Semiconductor Nanocrystal Quantum Dots. *Science* **2011**, *332,* 77-81.

(12) Geyer, S.M.; Allen, P.M.; Chang, L.-Y.; Wong, C.R.; Osedach, T.P.; Zhao, N.; Bulovic, V.; Bawendi, M.G. Control of the carrier type in InAs Nanocrystal Films by Predeposition Incorporation of Cd. *ACS Nano* **2010,** *4,* 7373-7378.

(13) Dalpian, G. M.; Chelikowsky, J. R. Self-Purification in Semiconductor Nanocrystals. *Phys. Rev. Lett.* **2006**, *96,* 226802-1–226802-4.

(14) Sahu, A.; Kang, M. S.; Kompch, A.; Notthoff, C.; Wills, A. W.; Deng, D.; Winterer, M.; Frisbie, C. D.; Norris, D. J. Electronic Impurity Doping in CdSe Nanocrystals. *Nano Lett.* **2012,** *12,* 2587–2594.

(15) Amit, Y.; Eshet, H.; Faust, A.; Patllola A.; Rabani, E.; Banin, U.; Frenkel, A. Unravelling the Impurity Location and Binding in Heavily Doped Semiconductor Nanocrystals: The Case of Cu in InAs Nanocrystals. *J. Phys. Chem. C* **2013**, *117,* 13688-13696.

(16) Amit, Y.; Li, Y.; Frenkel, A. I.; Banin, U. From Impurity Doping to Metallic Growth in Diffusion Doping: Properties and Structure of Silver-Doped InAs Nanocrystals. *ACS Nano* **2015**, *9,* 10790–10800.

(17) Martinez-Martin, D.; Longuinhos, R.; Izquierdo, J.G. ; Marele, A.; Alexandre, S.S.; Jaafar, M. ; Gómez-Rodriguez, J.M.; Bañares, L.; Soler, J.M. ; Gomez-Herrero, J. Atmospheric contaminants on graphitic surfaces. *Carbon* **2013**, *61,* 33-39.

(18) Giessibl, F.J. A direct method to calculate tip-sample forces from frequency shifts in frequency-modulation atomic force microscopy. *Applied Physics Letters* **2001,** *78,* 123.

(19) *see e.g*. Berger, J.; Spadafora, E.J.; Mutombo, P.; Jelínek, P.; Svec, M. Force-Driven Single-Atom Manipulation on a Low-Reactive Si Surface for Tip Sharpening. *Small* **2015**, *11,* 3686–3693.

(20) *For a review see* Kelvin Probe Force Microscopy. Editors Sascha Sadewasser and Thilo Glatzel *Springer* **2011**.

(21) Borowik, Ł.; Kusiaku, K.; Deresmes, D.; Théron, D.; Diesinger, H.; Mélin, T. Mapping charge transfers between quantum levels using noncontact atomic force microscopy. *Physical Review B* **2010,** *82,* 073302.

(22) Borowik, Ł.; Kusiaku, K.; Théron, D.; Mélin, T. Calculating Kelvin force microscopy signals from static force fields. *Applied Physics Letters* **2010,** *96,* 103119.

(23) Fuchs, F.; Caffy, F.; Demadrille, R.; Mélin, T.; Grévin, B. High-Resolution Kelvin Probe Force Microscopy Imaging of Interface Dipoles and Photogenerated Charges in Organic Donor−Acceptor Photovoltaic Blends. *ACS Nano* **2016**, *10,* 739-746.

(24) Borowik, Ł.; Nguyen-Tran, T.; Roca i Cabarrocas, P.; Mélin, T. Doped semiconductor nanocrystal junctions. *Journal of Applied Physics* **2013**, *114,* 204305.

(25) Jancu, J.M.; Scholz, R.; Beltram, F.; Bassani, F. Empirical spds* tight-binding calculation for cubic semiconductors: General method and material parameters, Phys. Rev. B **1998,** *57,* 6493.

(26) Delerue, C.; Lannoo, M., Nanostructures: Theory and Modelling (Springer, Berlin, **2004**)

(27) Delerue, C. Minimum Line Width of Surface Plasmon Resonance in Doped ZnO Nanocrystals, Nano Lett. **2017,** *17,* 7599.

(28) Hansen, W. N.; Hansen, G.J. Standard reference surfaces for work function measurements in air, *Surf. Sci.* **2001,** *481,* 172-184.

(29) Niquet, Y.M.; Delerue, C. ; Lannoo, M. ; Allan, G Single-particle tunneling in semiconductor quantum dots *Physical Review B* **2001**, *64,* 113305.

(30) Ebenstein, Y; Nahum, E; Banin, U. Tapping Mode Atomic Force Microscopy for Nanoparticle Sizing: Tip−Sample Interaction Effects. *Nano Letters* **2002**, *9,* 945–950.

(31) Fuchs, F.; Grévin, B.; Bocquet, F.; Nony, L.; Loppacher, C. Correct height measurements by Kelvin probe force microscopy: Poly(3-dodecylthiophene) on highly oriented pyrolytic graphite. *Physical Review B* **2013**, *88,* 205423.

(32) Geva, N.; Shepherd, J. J.; Nienhaus, L.; Bawendi, M. G.; Van Voorhis, T. Morphology of Passivating Organic Ligands around a Nanocrystal, *J. Phys. Chem. C* **2018**, *122, 45,* 26267-26274.

(33) Copie, G.; Biaye, M.; Diesinger, H.; Mélin, T.; Krzeminski, C.; Cleri, F. Deformation Localization in Molecular Layers Constrained between Self-Assembled Au Nanoparticles. *Langmuir* **2017,** 33, 2677–2687.

(34) Jacobs, H. O.; Leuchtmann, P.; Homan, O. J.; Stemmer, A. Resolution and contrast in Kelvin probe force microscopy, *Journal of Applied Physics* **1998,** *84,* 1168.

(35) Hostetler, M.J.; Wingate, J.E.; Zhong, C.J.; Harris, J.E.; Vachet, R.W.; Clark, M.R.; Londono, J.D.; Green, S.J.; Stokes, J.J.; Wignall, G.D., Glish,G.L.; Porter, M.D.; Evans, N.D.; Murray, R.W. Alkanethiolate Gold Cluster Molecules with Core Diameters from 1.5 to 5.2 nm: Core and Monolayer Properties as a Function of Core Size, Langmuir **1998,** *14,* 17-30.

(36) De Roo, J; Yazdani, N. Drijvers, E. Lauria, A.; Maes, J; Owen, J.S.; Van Driessche, I.; Niederberger, M.; Wood, V.; Martins, J.C.; Infante, I.; Hens, Z. Probing Solvent–Ligand Interactions in Colloidal Nanocrystals by the NMR Line Broadening, Chem. Mater. **2018,** *30,* 5485–5492.

TOC GRAPHIC

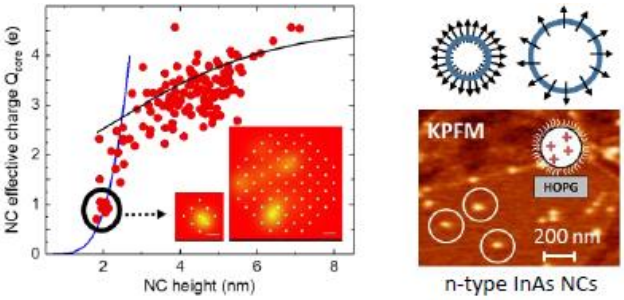
NC effective charge Q_{core} (e)
NC height (nm)
KPFM
HOPG
200 nm
n-type InAs NCs